Applied Soft Computing 52 (2017) 247–261

Contents lists available at ScienceDirect

Applied Soft Computing

journal homepage: www.elsevier.com/locate/asoc

Detection and sizing of metal-loss defects in oil and gas pipelines using pattern-adapted wavelets and machine learning

Mohamed Layouni[a,b,*], Mohamed Salah Hamdi[a], Sofiène Tahar[b]

[a] Ahmed Bin Mohammed Military College, P.O. Box 22713, Doha, Qatar
[b] Concordia University, Electrical & Computer Engineering Department, 1455 de Maisonneuve Blvd. W, Montreal, Quebec, Canada H3G 1M8

ARTICLE INFO

Article history:
Received 7 May 2014
Received in revised form 26 October 2016
Accepted 27 October 2016
Available online 8 November 2016

Keywords:
Oil and gas pipelines
Safety assessment
Pattern-adapted wavelets
Pattern recognition
Neural networks
Machine learning
Defect location
Defect sizing
Magnetic flux leakage

ABSTRACT

Signals collected from the magnetic scans of metal-loss defects have distinct patterns. Experienced pipeline engineers are able to recognize those patterns in magnetic flux leakage (MFL) scans of pipelines, and use them to characterize defect types (e.g., corrosion, cracks, dents, etc.) and estimate their lengths and depths. This task, however, can be highly cumbersome to a human operator, because of the large amount of data to be analyzed. This paper proposes a solution to automate the analysis of MFL signals. The proposed solution uses pattern-adapted wavelets to detect and estimate the length of metal-loss defects. Once the parts of MFL signals corresponding to metal-loss defects are isolated, artificial neural networks are used to predict their depth. The proposed technique is computationally efficient, achieves high levels of accuracy, and works for a wide range of defect shapes.

1. Introduction

Oil and gas pipelines are an important component of the energy sector nowadays. In the US, 70% of all petroleum transported in 2009 was carried by pipeline [4]. In Canada, 97% of all natural gas and crude oil production is currently being transported by pipeline [14]. However, despite being considered as one of the safest and cheapest ways to transport oil and gas [13,14], pipelines are still prone to a variety of metal-loss defects such as corrosion, cracks, and dents. These defects are mainly due to factors, such as extreme temperature and pressure inside the pipeline, exposure to highly corrosive chemicals, water, etc. The repercussions of not detecting and repairing such defects on time can be very serious: huge financial losses, damage to the environment, health and life hazards, etc. Given the size of an average pipeline, and the amount of data generated from magnetic scans, relying on human operators to sift through the data and find defects is a highly challenging and error-prone task.

This paper describes a solution to automate the process of inspecting MFL data [16–18] generated through the scanning of oil and gas pipelines. The proposed solution uses a technique based on *pattern-adapted wavelets* [15,36] to detect, locate, and estimate the length of metal loss defects along the pipeline. Once a defect is located, a number of features are extracted from the corresponding MFL signal. Those features are then fed into an artificial neural network which returns an estimate of the defect depth. The obtained depth and length are then used to assign a severity rating to the detected defect, and decide whether or not urgent repairs are due. The severity rating is assigned using industry standards such as ASME.BG31 [3], which provides a formula to evaluate a defect's severity given its dimensions, the operating pressure inside the pipeline, and other properties of the steel used to build the pipeline.

Related work. The development of techniques to assess the safety of oil and gas pipelines has attracted the attention of many researchers over the last several years [17,18,46,41,51,20,39,50]. Results on this topic are very diverse in terms of what they achieve, the specific problems they address, and the approaches they use. Fig. 1 provides a high-level summary of the research landscape in this area. Following the notation in Fig. 1, we can divide the literature on this topic into three main groups:

* Corresponding author. Tel.: (+1) 514 848 2424.
E-mail addresses: layouni@ece.concordia.ca (M. Layouni), mshamdi@abmmc.edu.qa (M.S. Hamdi), tahar@ece.concordia.ca (S. Tahar).

http://dx.doi.org/10.1016/j.asoc.2016.10.040
1568-4946/

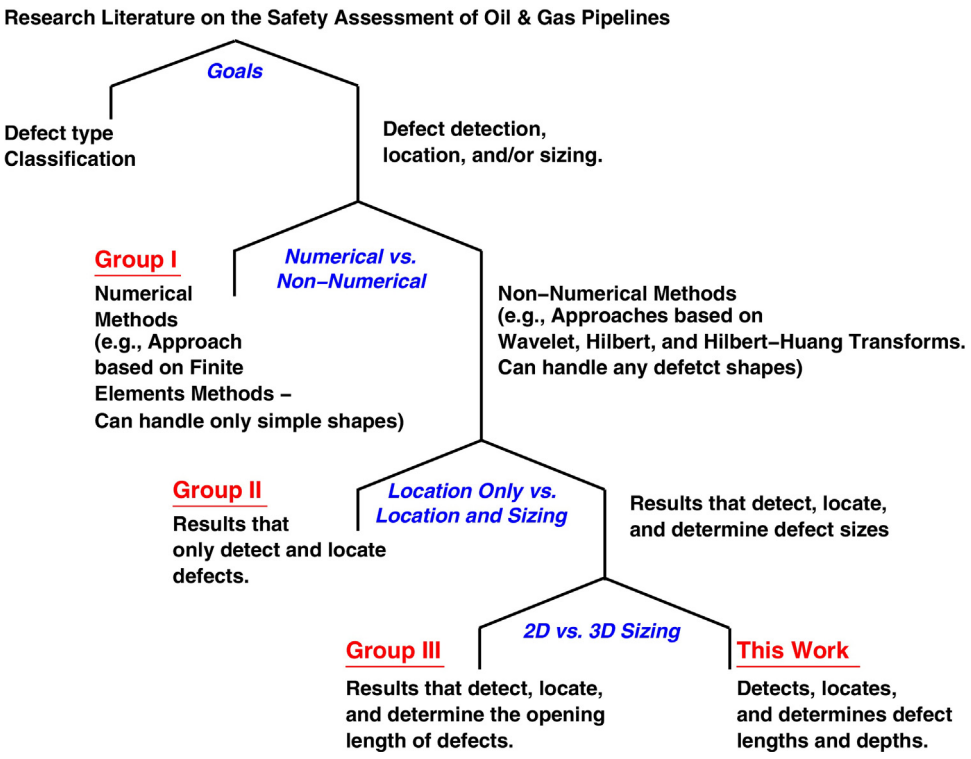

Fig. 1. Summary of related work and comparison to this paper.

Group I. Numerical techniques to determine defect sizes.

Group II. Non-numerical techniques to detect and locate defects (sizing problem not considered).

Group III. Non-numerical techniques to detect, locate, and determine the opening length of defects. Some of the work in this category does also provide ways to classify defects and other pipeline features into different types (e.g., holes, valves, junctions, etc.).

It is worth noting at this point that work listed under Groups II and III includes cases where the application domain is not related to oil and gas pipelines. Some of the techniques, for example, relate to the detection and location of defects in underground power cables. In some cases also, the signals being analyzed are not MFL signals (e.g., electrical, acoustic, and pressure wave signals). None of the non-numerical methods found in the literature considered the problem of determining defect depths.

In the following, we summarize each of the group of techniques listed above, and show the similarities and differences with the work in this paper.

Group I: Numerical techniques to determine defect sizes. The work in [17,18,46] considered numerical methods, not based on wavelets, to address the problem of defect sizing from MFL signals. These methods however only apply to defect shapes for which analytical models are known. The approach proposed in [17,18,46] is to express the relationship between MFL signals and defect geometries through an equation of the form:

$$\mathbf{B}_{\mathrm{MFL}} = \mathbf{F}(\mathbf{D}) \tag{1}$$

where $\mathbf{B}_{\mathrm{MFL}}$ denotes the MFL signals, $\mathbf{D}$ denotes the defect geometry, and $\mathbf{F}(\cdot)$ denotes the analytical model describing the behavior of the MFL signals in relation to the defect geometry. Determining the size of a defect, then, reduces to inverting Equation (1) and finding $\mathbf{D}$ given $\mathbf{B}_{\mathrm{MFL}}$ and $\mathbf{F}(\cdot)$. This approach is straightforward, but has a number of limitations: (i) Eq. (1) may have several solutions, which could lead to several plausible defect geometries; (ii) solving Eq. (1) has a high computational cost – at least cubic in the size of the MFL signals matrix $\mathbf{B}_{\mathrm{MFL}}$ [29]; and (iii) the analytical model $\mathbf{F}(\cdot)$ itself is not always available. In fact, apart from a limited number of simple defect shapes (e.g., cylindrical, spherical, spheroidal, and cuboidal [18,46,29]), analytical models for general arbitrary defect shapes are still hard to derive [18,46]. This is due to the fact that deriving analytical models requires solving Maxwell's equations of magnetism [1], which is not easy for defects of general arbitrary shapes.

The authors in [17,18,46] demonstrate their approach on a number of simple defect shapes, and solve the sizing problem using techniques such as the finite element method (FEM) [48], linear algebra, and machine learning. However, as explained above, it is hard to apply this approach to defects of arbitrary shapes.

More recently, the authors in [42] have used numerical methods to study the relationship between MFL signals and defect geometries (length and depth). They conclude their paper by confirming the non-linear nature of the relationship between MFL signals and defect geometries. They do also point out the difficulty of using numerical methods for determining defect depths from MFL signals, since several defect geometries can lead to the same MFL signal characteristics (e.g., maximum peak amplitude).

Building on the observations of [42], the work in [44] uses numerical methods to estimate the worst-case defect depth corresponding to a given MFL signal. The proposed method is applied to an MFL model generated from a non-linear FEM approximation. The authors conclude by pointing out that the accuracy of the worst-case defect depth depends on the quality of the MFL model being used, and that for defects deeper than 70% of the wall's thickness, the solutions found by their method may not be correct.

Finally, the work in [27] describes a model to estimate defect depths as a quadratic function of the MFL peak values. The parameters of the model, however, are obtained by computing an FEM approximation of the MFL field for a given defect shape. The experimental results reported by the authors show that their method

achieves an estimation error of less than 20% of the pipeline wall's thickness, which is acceptable by industry standards. The main limitation of [27] is that it relies on FEM-derived analytical models, which can be obtained only for simple defect shapes.

The work presented in this paper does not require analytical models, and uses pattern-adapted wavelets [36,37] and machine learning techniques [22,38] that can be applied to any defect shapes.

Group II: Non-numerical techniques to detect and locate defects (no sizing). The authors in [41,51] have used wavelets for the purpose of de-noising MFL signals, as well as detecting, and locating defects oil and gas pipelines. The problem of defect sizing however was not considered by these authors.

Wavelets have also been used in other applications, including the detection and characterization of faults in underground power cables [31,35,25,6]. More precisely, the authors in [31,35,25,6] have used wavelet transforms to detect and locate faults, and classify them into a set of predefined fault types. The work in [31,35,25,6] is related to this paper, but there are two important differences. In particular, the work in this paper models defects as 3D objects, and uses wavelets both to locate them and determine their sizes, while the work in [31,35,25,6] does not consider the sizing problem, since it models faults as discrete points on a line. Moreover, the work in [31,35,25,6] uses general purpose mother wavelets, whereas this paper uses a customized mother wavelet adapted to the reference pattern to be detected.

Wavelets [37] have also been used previously in the area of biology, for example, to detect various health problems, such as brain and heart illnesses [36,2,19]. Their usage in biology, however, was only to detect anomalies, and not to quantify them. In other words, the problems considered in [2,19] are mainly detection problems: i.e., the goal was to analyze signals from biological measurements, and determine which parts of the signals are normal, and which ones are abnormal.

Group III: Non-numerical techniques to detect, locate, and determine the opening length of defects. The authors in [9,39,50] have used wavelets to analyze other types of signals, namely pressure wave signals inside a pipeline, for the purpose of detecting and locating holes and other features (e.g., valves, junctions) in a pipeline network. The work in [20] uses similar signal processing methods, namely, the Hilbert transform (HT) [45] and Hilbert–Huang transform (HHT) [45], to detect and locate holes from pressure wave signals.

The solutions proposed in [9,20,39,50] rely on the following physical phenomenon. A leaking hole causes a local change in density in the fluid flowing inside the pipeline, which in turn provokes reflections in the pressure wave signal. These reflections can be detected as echoes. The techniques in [9,20,50] infer the location of the defect from the time it takes for echoes to arrive at some appropriately placed sensor. The solutions in [9,50] use two noise-filtering techniques (Kurtosis [5] and Cepstrum [11]) to make it possible to recognize echoes in the wavelet transform, despite high levels of noise in the pressure wave signals.

The work in [39] assumes a slightly different setting, where two sensors are placed at two different locations on the pipeline, such that the distance between the two is known. The pipeline is then excited with a pressure wave, which propagates through the fluid inside the pipeline, and produces a reflexive wave when encountering a hole. The technique in [39] estimates the time difference it takes for the reflexive wave to arrive at each sensor. Given this time difference and the wave speed, the authors in [39] infer the location of the defect. The work in [39] conducts a fine-grained analysis of the wave speed of direct waves (non-dispersive waves) and the reflective waves (dispersive waves), thereby achieving higher precision than earlier methods based on cross-correlation between the signals received at each sensor [40,8].

While related, there are some important differences between the work presented in this paper and those in [9,20,39,50].

1. First, the goal of this paper is to detect not only holes and leaks, but also defects that do not lead to a hole in the pipeline wall. This includes for example, superficial metal-loss defects from corrosion, or construction defects inside the pipeline wall (i.e., an air gap inside the wall of the pipeline that does not show any features on the external surface of the pipeline wall). In the case of a superficial metal-loss (e.g., from corrosion), it is not clear if the resulting echoes in the pressure wave signals would be important enough to be detected. For construction defects (i.e., air gaps inside the pipeline wall), it is clear that pressure wave signals cannot detect their presence. These two types of defects, as well as holes, are however detectable using MFL signals. This is probably the reason why MFL scanning is the most widely used inspection method in the oil and gas industry.
2. The authors in [39] indicate also that the method they propose is not applicable to pipelines carrying incompressible fluids such as crude oil because the used technique relies on a particular behavior of vibro-acoustic waves in compressible fluids such as gas. The MFL signals used in this paper do not have this constraint, and work on any type of metallic pipelines regardless of the fluid or gas they carry.
3. Moreover, the method proposed in this paper provides an estimate of the opening length and depth of a defect, and not only its location. By contrast, the technique in [39] is mainly intended for locating hole defects. However, that technique could be used to infer the opening length of a defect, if the location of each edge of a defect is determined.
4. The work in this paper uses wavelets for a completely different purpose than [9,39,50]. For instance, the work in [9,50] use the wavelet transform to filter out noise from pressure wave signals (which will be further analyzed to find "spikes" in amplitude, or echoes, whose coordinates indicate the location of holes on the pipeline). This work on the other hand uses wavelet transforms to locate the occurrence of a possibly dilated version of a reference pattern in the MFL signals. Such an occurrence causes a local maximum in the Wavelet Transform. This is possible, because the mother wavelet in this paper is built from the pattern signal of the defect to be detected.[1] The solutions in [9,39,50] on the other hand, use generic mother wavelets (Morlet and the Mexican Hat), either to filter noisy signals, or to detect peaks in the wavelet transform; the latter correspond to the arrival time of reflected echoes.
5. Finally, the work in [20] uses Hilbert transform (HT) and Hilbert–Huang transform (HHT) to analyze pressure wave signals. While the patterns being detected in [20] are different from the ones in this paper, further research needs to be done to see how those signal processing techniques can be applied to MFL signals. The question of estimating defect sizes (opening length and depth) using the techniques in [20] needs to be further explored as well.

Summary of paper contribution. This paper presents a technique to detect and locate defects in MFL data, and determine their lengths and depths. The proposed technique is based on pattern-adapted wavelets [36,37] and machine learning [22,38]. The solution in this paper does not rely on analytical models, and can detect the occurrence of any reference pattern in the MFL signal. As a result, the proposed technique can handle a wide range of defect shapes, even those for which no analytical models are

[1] More details on the use of pattern-adapted wavelets are given in Section 3.2.

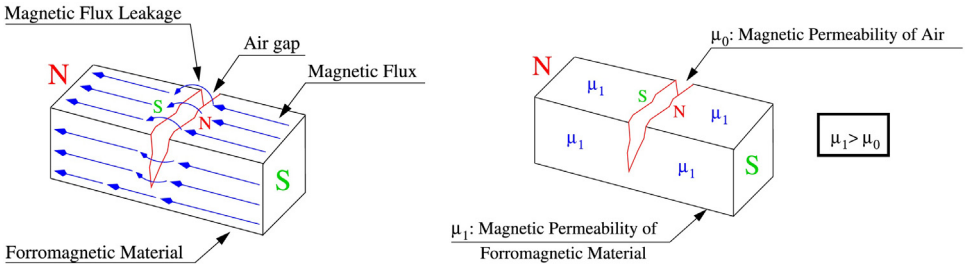

(a) Magnetic Flux Leakage around a defect

(b) Magnetic permeability in air and steel

Fig. 2. Magnetic flux leakage.

known. Unlike related work in Groups II and III, this paper presents a technique to estimate defect depths from MFL signals.

Paper outline. The remainder of this paper is organized as follows. Section 2 gives a brief overview on MFL scanning, and highlights the main idea behind its use in the detection of metal-loss defects. Section 3 introduces wavelets and shows how they are used to locate defects and estimate their length. Section 4 describes the features extracted from the MFL signals of detected defects, and the artificial neural network built to analyze them. It also presents the performance results and compares them to those achieved by the linear regressions technique. Section 6 provides a summary, and discusses the performance of the overall solution. Finally, Section 7 provides concluding remarks and ideas for extending this work.

2. MFL-based pipeline inspection

MFL scanning is a well established technique for inspecting pipelines made from ferromagnetic material [3]. The technique makes it possible to detect, locate, and estimate the size of metal loss defects present on a pipeline. The idea behind MFL scanning is the following. When two strong magnets of opposite polarity are held close to the surface of a pipeline, the latter is magnetized, and lines of magnetic force flow through the walls of the pipeline, from the south pole to the north pole. When the pipeline wall contains a crack or a thinning (due to corrosion, for example), two new poles appear at the edges of the crack: a north pole and a south pole, similar to when a magnet is broken in two. As a result, the magnetic lines of force now flow through the ferromagnetic material of the pipeline wall, then through the air gap created by the crack, then again through the ferromagnetic material (Fig. 2a). The set of magnetic lines of force flowing through these materials (e.g., ferromagnetic steel, air) is called magnetic flux. And the density of magnetic flux in each material depends on a physical property of the material called *Magnetic Permeability*. Informally speaking, the Magnetic Permeability of a given material denotes the degree to which magnetic flux is able to flow through that material. This is very similar to the concept of conductivity in electricity, or fluid permeability in porous materials such as rocks.

Different materials have different magnetic permeability. For instance, ferromagnetic steel has a much higher magnetic permeability than air. Therefore, the density of magnetic flux in the healthy parts of the pipeline is much higher than the density of magnetic flux in the air gap created by the crack (Fig. 2b). As a result, the magnetic lines of force bulge out as they go through the air gap, because air cannot absorb as much flux per unit volume as the ferromagnetic material of the pipeline. This bulging of magnetic flux is called *Magnetic Flux Leakage*; it is the physical phenomenon the pipeline industry relies on to detect defects in oil and gas pipelines. Fig. 2a illustrates the magnetic flux leakage phenomenon.

In MFL-based inspection, a scanning tool equipped with strong magnets and magnetic sensors is sent inside a pipeline. The walls of the pipeline are magnetized, and sensors are used to measure any magnetic flux leakage. The sensors are equally-distributed around the circumference of the pipeline, and move with the inspection tool parallel to the axis of the pipeline. The use of several sensors around the circumference of the pipeline makes it possible to precisely locate the angular position of a defect. Fig. 3 shows a rolled-out representation of the pipeline, and how the MFL sensors are equally spaced along the *x*-axis, above the pipeline. Any magnetic flux leakage detected by the sensors indicates the presence of a defect. The MFL signals measured by the sensors are recorded, and later analyzed to locate possible defects, and determine their sizes and severity levels. MFL signals are the main input data to the solution presented in this paper.

3. Pattern-adapted wavelets for the detection and sizing of metal-loss defects

3.1. MFL signal patterns around defect edges

MFL signals recorded in the neighborhood of a metal-loss defect have a distinct shape. Figs. 4 and 5 show sample MFL signals simulated for cylindrical and cuboidal defects, respectively. Fig. 5 displays the individual MFL signals simulated for each of the sensors passing above the defect. The *X* and *Y* axes in Figs. 4 and 5, as

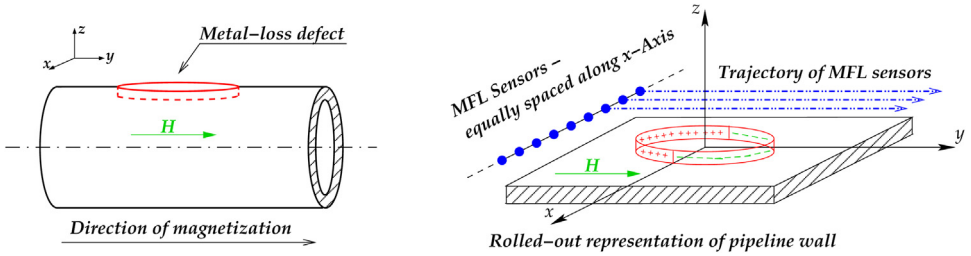

Fig. 3. MFL measurement setting.

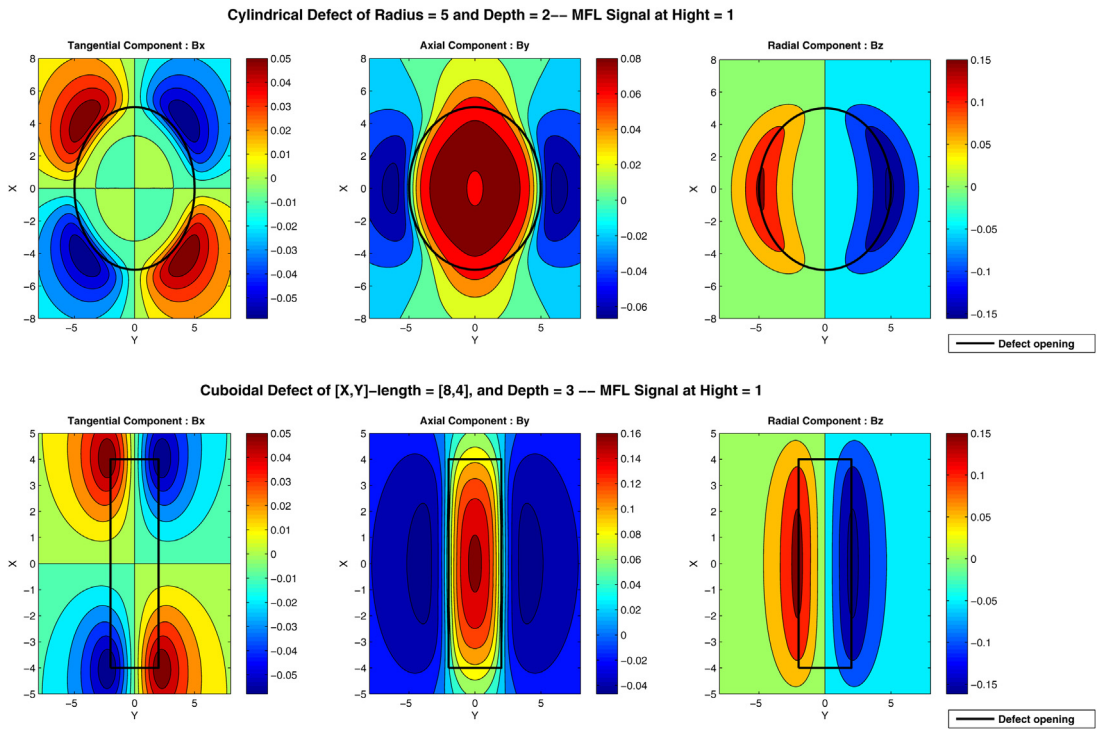

Fig. 4. MFL scan of cylindrical (top) and cuboidal (bottom) defects.

well as the sensors trajectories and direction of magnetization, are as indicated in Fig. 3. The MFL signals in Figs. 4 and 5 were simulated in MATLAB [34] using analytical models described in [16–18,29].

As can be seen in Fig. 4, the sensor passing directly above the center of the defect (i.e., along $x = 0$) has the MFL signal for which the axial and radial components have the highest amplitude. This amplitude gets lower for sensors further away from the center of the defect. The MFL signals of other regularly-shaped defects (such as spheroidal and spherical defects) have patterns similar to the ones in Figs. 4 and 5.

As can be noted in Figs. 4 and 5, MFL signals show a distinct behavior around defect edges. For example, peaks in the tangential and radial components (B_x and B_z) of the MFL signal mark the location of defect edges. The technique proposed in this paper uses the MFL behavior around metal-loss defects as a reference pattern. The next subsection explains how this reference pattern is used in

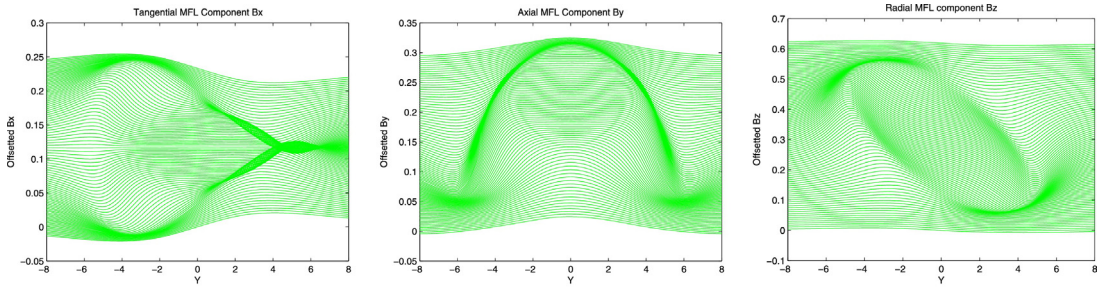

(a) Cylindrical defect of Radius = 5 and Depth = 2 (length units)

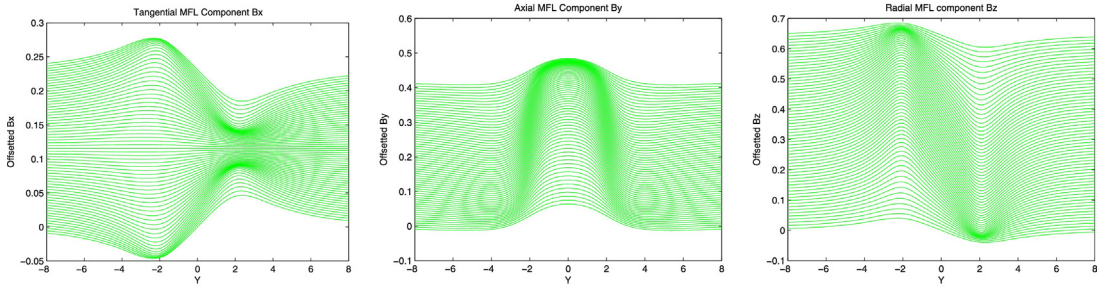

(b) Cuboidal defect of Length $L_X = 8$, Width $L_Y = 4$, and Depth = 3 (length units)

Fig. 5. MFL signals from each of the sensors passing above a defect.

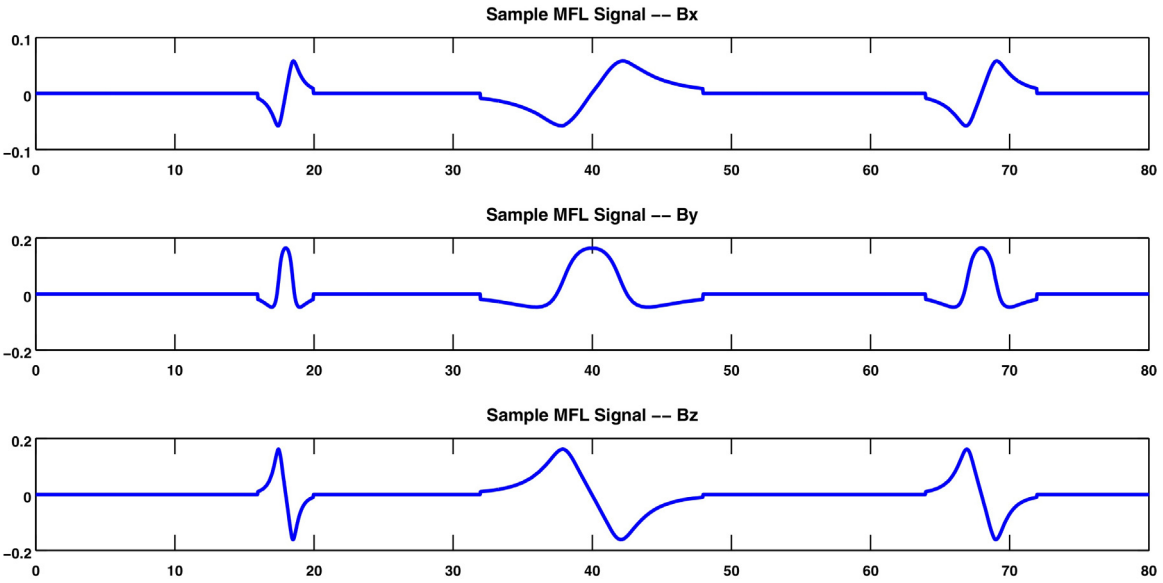

Fig. 6. Sample MFL scan of a pipeline with three metal-loss defects of cuboidal shape.

connection with wavelet transforms to automate the detection and location of defect edges.

3.2. Wavelets as a technique to represent and analyze signals

Wavelets are a powerful mathematical tool with a wide variety of applications ranging from high-efficiency data compression [12] to data analysis and classification [9,39,41,49–51]. Informally speaking, a wavelet transform provides a mechanism to compute the degree of similarity a signal and reference pattern. There is a rich body of work in the literature detailing the theoretical foundations of wavelets [15,32,37]. For the purpose of this paper, however, only a few important facts about wavelets are highlighted.

For a signal $f(x)$, the wavelet transform of f, with respect to mother wavelet $\psi(x)$, is defined as:

$$\begin{aligned}(Wf) &: \mathbb{R}^{+*} \times \mathbb{R} \longrightarrow \mathbb{C} \\ (a,b) &\longmapsto (Wf)(a,b) = \int_{-\infty}^{\infty} f(x)\psi_{a,b}(x)dx \end{aligned} \tag{2}$$

where $\psi_{a,b}(x) \equiv |a|^{1/2}\psi(a(x-b))$.

For a function $\psi(x)$ to be an admissible mother wavelet, it is sufficient that the following conditions [37,15] be satisfied:

$$\psi(x) \text{ is real}, \quad \psi(x) \in L^1 \cap L^2, \quad x\psi(x) \in L^1, \quad \text{and}$$

$$\int_{-\infty}^{\infty} \psi(x)dx = 0 \tag{3}$$

where L^1 and L^2 denote the space of integrable and square integrable functions over $\mathbb{R}$, respectively.

Following are a few important properties of the wavelet transform.

- The mother wavelet, which is chosen in the setup phase, specifies the reference pattern of the wavelet transform.
- The parameters a and b in the wavelet transform $(Wf)(a,b)$ denote the width of the pattern being tested, and the location where the pattern is centered, respectively.
- A local maximum in the wavelet transform at coordinates (a_0, b_0) indicates the presence of an instance of the reference pattern of width a_0, at location b_0.

Fig. 6 shows a sample MFL signal from a pipeline containing three defects of cuboidal shape. The reference patterns used to detect those defects are shown at the top of Fig. 7. Since these patterns do not necessarily satisfy the admissibility conditions in (3), they cannot be used directly as mother wavelets. The mother wavelets are constructed instead as an approximation of the reference patterns. Following is a description of the procedure. Let f denote a reference pattern, such that f is a square integrable real function with a compact support. Let $[u, v]$ denote the interval

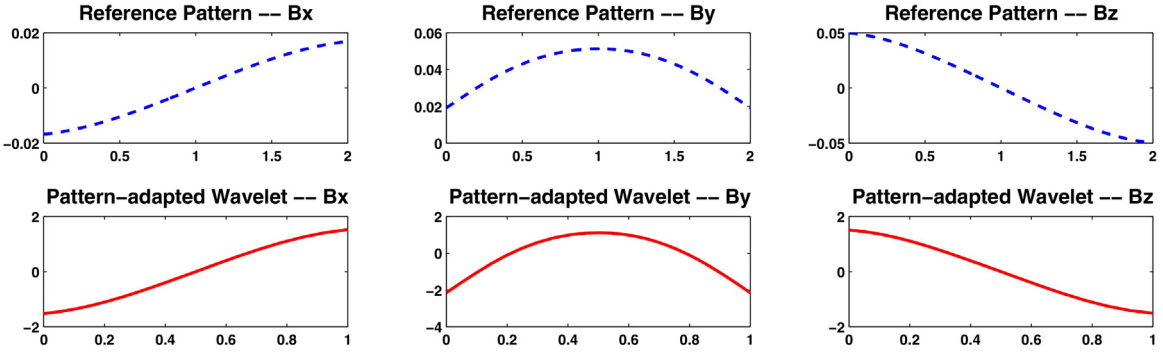

Fig. 7. Reference patterns and admissible mother wavelets for defects of cuboidal shape.

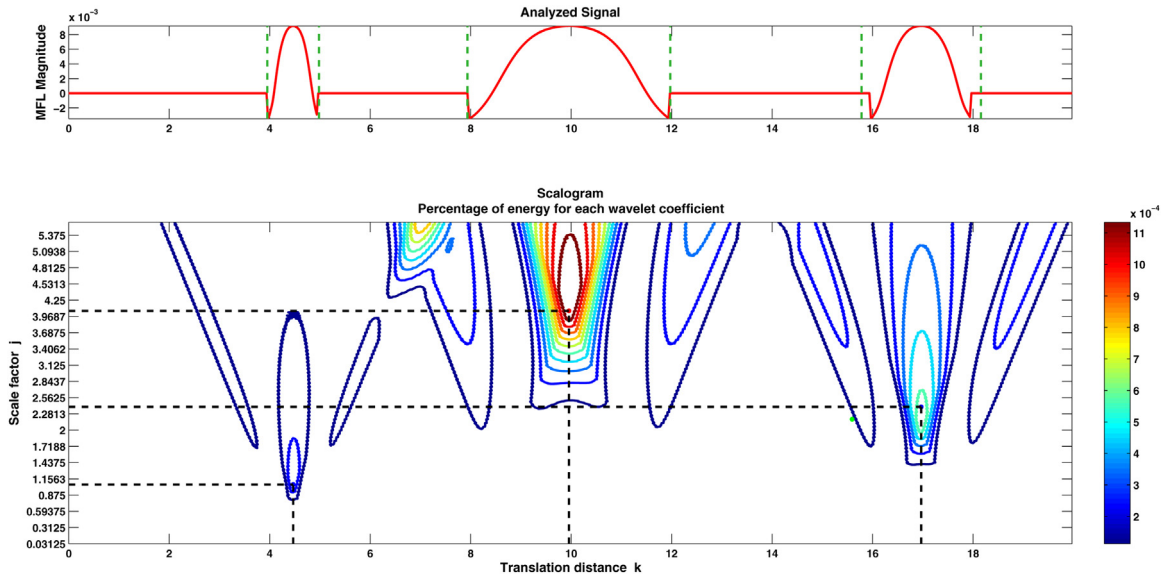

Fig. 8. Wavelet transform of an MFL signal with respect to a pattern-adapted wavelet basis.

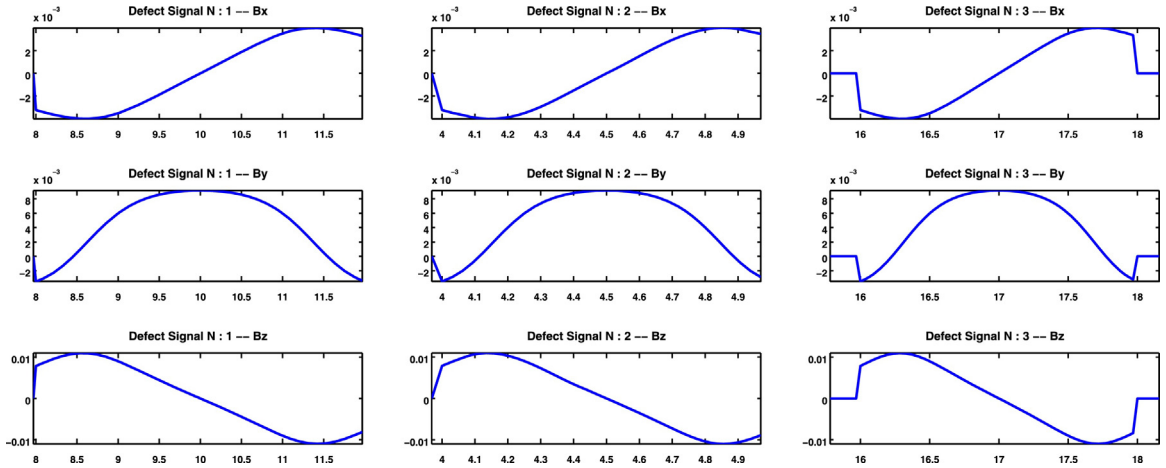

Fig. 9. Portions of the MFL signal in Fig. 8 corresponding to metal-loss defects.

containing the support of f. Let $\hat{\psi}$ be the function defined as: $\hat{\psi} : [u, v] \longrightarrow \mathbb{R}, x \longmapsto f(x) - (1/(v-u)) \times \int_{\mathbb{R}} f(x)dx$. It can be easily seen that the function $\hat{\psi}$ defined above satisfies the admissibility conditions stated in (3). The mother wavelet ψ is finally chosen as a normalized version of $\hat{\psi}$. That is

$$\begin{aligned} \psi : [u, v] &\longrightarrow \mathbb{R} \\ x &\longmapsto \frac{\hat{\psi}(x)}{\|\hat{\psi}\|} = \frac{\hat{\psi}(x)}{\sqrt{\int_{\mathbb{R}} \hat{\psi}^2(x)dx}} \end{aligned} \tag{4}$$

The function ψ is an admissible mother wavelet. Moreover, it is adapted to the reference pattern f, and preserves its shape.

The computation of the pattern-adapted mother wavelet ψ has been performed in practice using the `pat2cwav` function provided in the Matlab Wavelet Toolbox [34]. Additional methods for constructing pattern-adapted wavelets can be found in [37].

Fig. 8 shows the y-component of an MFL signal with three defects (top) and its wavelet transform (bottom). The coordinates of the local maxima in the wavelet transform are highlighted. The horizontal coordinates indicate the center of the detected defects, while the vertical coordinates are used to determine the width of each defect.

Fig. 9 shows fragments from the MFL signal of Fig. 8, corresponding to the detected metal-loss defects. All three components (B_x, B_y and B_z) of the MFL signal are given. It can be easily seen how these signals are dilated and translated versions of the reference patterns shown in Fig. 7.

The same method is applied to a noisy MFL signal with a signal-to-noise ratio[2] (SNR) = 10 dB. The results of the detection and the signal fragments corresponding to the detected defects are shown in Figs. 10 and 11, respectively. The level of precision achieved at locating defects and estimating their lengths, both for noisy and noiseless signals, demonstrates the robustness of the method.

The extracted signal fragments (Figs. 9 and 11) will be further analyzed to estimate the depth of the detected defects. This is described in Section 4.

[2] $\mathrm{SNR} \equiv 10 \log_{10}(P_{\mathrm{Signal}}/P_{\mathrm{Noise}})$, where P denotes power.

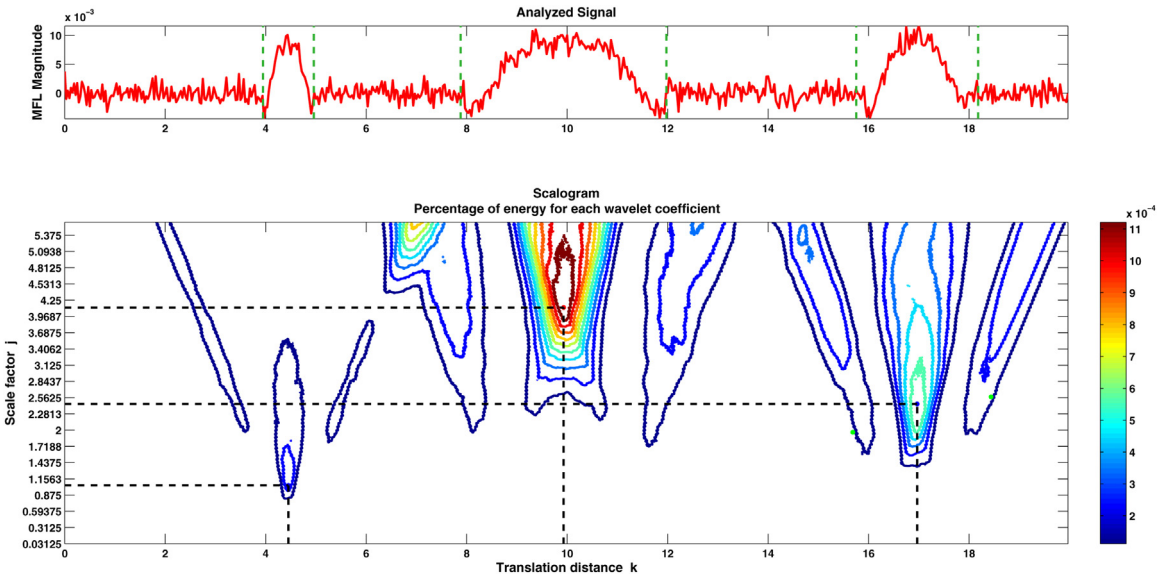

Fig. 10. Defect detection in MFL signal with White Gaussian Noise (SNR = 10 dB).

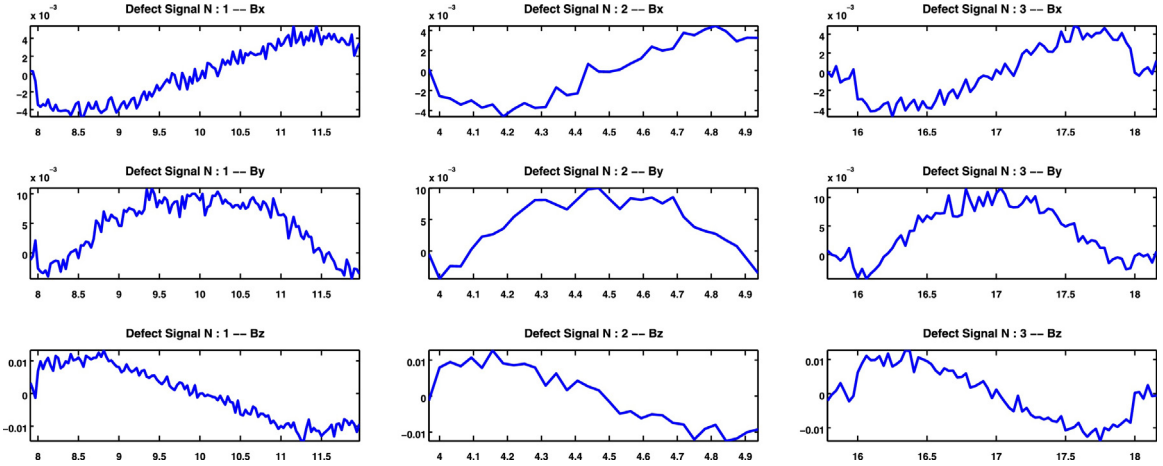

Fig. 11. Portions of the MFL signal in Fig. 10 corresponding to metal-loss defects.

4. Artificial neural network to estimate defect depths

4.1. Motivation

Depth and length are very important factors to determine the severity of a metal-loss defect. Industry standards, such as ASME B31G-1991 [3], provide criteria (c.f., Fig. 12) to determine the severity of a defect from its length and depth, given information such as the operating pressure, and the physical properties of the material from which the pipeline is made. Defect lengths were determined in the previous section. This section will focus on finding defect depths.

By observing the MFL signals of metal-loss defects it can be noted that the magnitude of the signals is much higher for defects with larger depths. Fig. 13 shows, for instance, the MFL signals of two cylindrical defects with the same radius, and depths 0.1 and 1.2 length units, respectively.[3] As can be seen in Fig. 13, the magnitude of the MFL signals of the defect of depth 1.2 is about 10 times higher than those of the defect of depth 0.1. The relationship between defect depths and the magnitude of MFL signals is not a linear one, however. In fact, this relationship is still not well understood, and defect depths may depend on other features of the MFL signal.

A lot of research has been dedicated to understanding the relationship between MFL signals and defect depths [46,16–18], but the problem unsolved to this day. The work in [18] gives a number of arguments as to why analytical models expressing depth as a function of the MFL signal cannot always exist. Following the arguments in [18], this work explores the use machine learning techniques to predict defect depths from MFL signals.

The focus of this work is not to find the best possible machine learning (ML) technique for the task, but rather to find a technique that gives reasonably good results. Artificial neural networks (ANN) [22] have been chosen as a candidate ML technique because of their generality and ability to learn complex relations. For comparison purposes the prediction task was also performed using linear regression [22].

4.2. Overview on artificial neural networks

Artificial neural networks (ANNs) [22] are a popular algorithmic tool that attempts to mimic the architecture of neural networks in the human brain. ANNs have proved to be effective in a variety of

[3] The locations of the zero-crossings in the B_y graph of Fig. 13 indicate the actual limits of the defect opening.

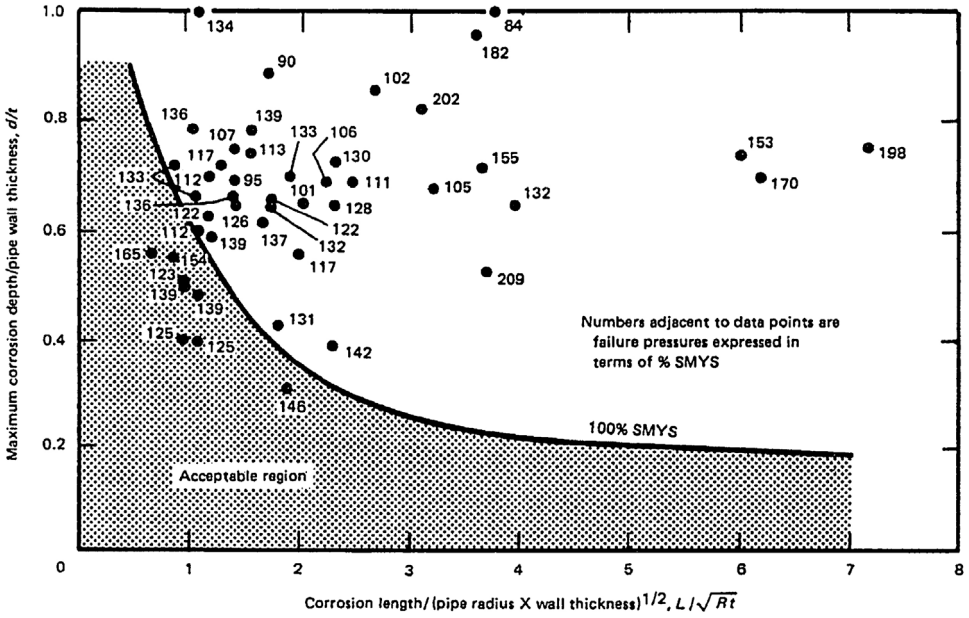

Fig. 12. Parabolic criteria for classifying corrosion defects based on length and depth, for a given pipeline material and operating pressure [3].

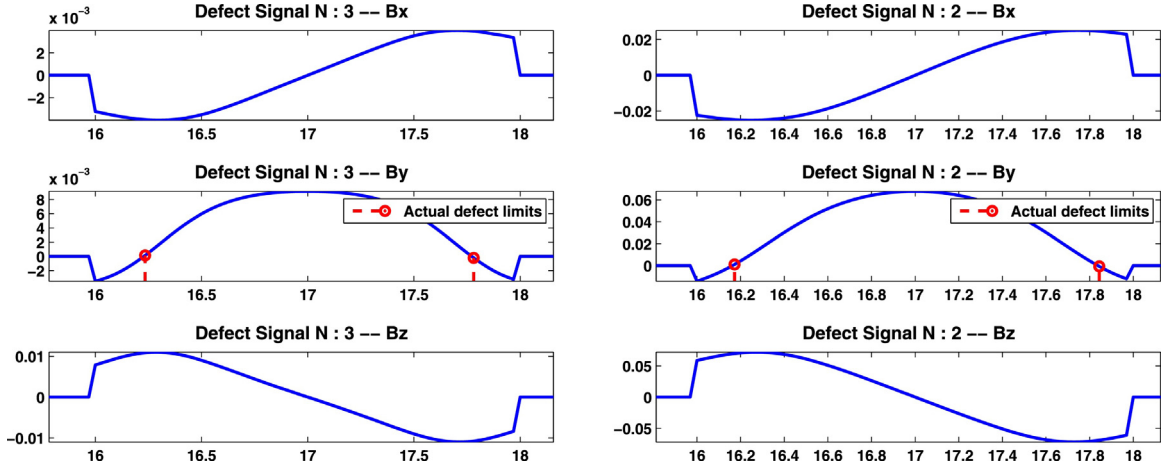

Fig. 13. Difference in MFL magnitude for cylindrical defects of same radius and different depths.

tasks such as data fitting, function approximation, time series prediction, data classification, data clustering, etc. Generally speaking, ANNs can be thought of as a computational tool capable of approximating a function having multiple inputs and outputs. It consists of a graph of neurons linked to each other by edges. Each neuron computes a function (called Activation function) on the values received on its input edges, and sends the result forward on its output edge. In addition, each neuron N_i in the network has a bias b_i, and each edge linking neuron N_i to N_j has a weight W_{ij}. Let $A_i()$ denote the activation function of neuron N_i, and let $I_{i1}, \ldots, I_{ik}$ denote its inputs. The output of neuron N_i is computed as $O_i = A_i(b_i + \sum_{j=1}^{k} W_{ij} I_j)$. Fig. 14 shows an example of an artificial neural network.

The network of neurons described above is augmented with a search algorithm that determines the optimal weights and biases that minimize the error between the final output of the network, and the output of the function to be approximated. Let F denote the function to be approximated. The search for the optimal weights and biases is an iterative process that loops through pairs of input–output data $\{(X_\ell, F(X_\ell)), \ell \in [1, M]\}$, and adjusts the weights and biases so that the output of the network on inputs X_ℓ is closer to $F(X_\ell)$. This phase, when the network parameters are being adjusted, is called the training phase, and the set of pairs $\{(X_\ell, F(X_\ell)), \ell \in [1, M]\}$ is called the training data. When the training phase is complete, the resulting neural network can be used to predict F on fresh input data.

ANNs have been applied in a variety of fields, ranging from robotics [21], to data science [10], to medicine [2,26], and financial

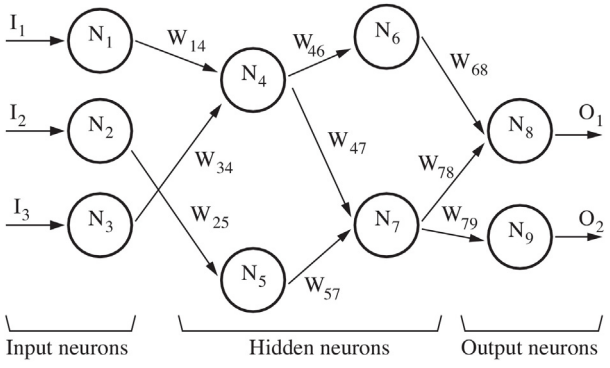

Fig. 14. Structure of an artificial neural network.

Table 1
Number of principal components for noisy and noiseless data sets.

	Noiseless	SNR = 10 dB	SNR = 5 dB	SNR = 3 dB
Number of principal components explaining 95% of the variance in the data	7	8	9	10

markets forecasting [28]. More details about ANNs can be found in [22].

4.3. Preparing the dataset

Raw MFL signals are vectors of arbitrary sizes and cannot be fed directly to the ML techniques considered in this work. Instead, various features are first extracted from the signals and then used to build a dataset. The next section discusses the choice of features, and describes the feature extraction procedure.

4.4. Extracting features from MFL signals

There are many possible features that can be extracted from a given signal. These can range from characteristics such as maximum magnitude and peak-to-peak distance, to metrics such as mean-average and standard deviation. The goal, however, is to compute the smallest set of features that captures most of the information contained in the signal. Ideally, one should be able to regenerate the signal right from the extracted set of features, while keeping the latter small.

In this work, the following features were extracted because of their apparent dependence on the defect depth.

- maximum magnitude,
- peak-to-peak distance,
- mean average,
- standard deviation,
- integral of the normalized signal.[4]

The above features do capture a lot of the information contained in the signals, but not everything. To make sure, the maximum amount of information about the signal is captured, polynomial series were used to approximate the MFL signals. For this particular instance of the MFL signals, polynomials of degrees 3, 6, and 6 provided the best approximation for B_x, B_y, and B_z respectively. By convention, a degree n polynomial is written $P(X) \equiv a_n X^n + \cdots + a_1 X + a_0$. The coefficients of the polynomial approximations, along with the above features, give a total of 33 features ($33 = (5 \times 3) + 4 + 7 + 7$). To reduce the number of features and remove redundancy, principal component analysis (PCA) [24,23] was conducted on the data set. Table 1 gives the final number of features for noisy and noiseless MFL signals. The initial dataset (with 33 features) is projected along the principal components obtained through PCA, and the result is fed to a machine learning algorithm.

Two machine learning techniques are considered in this paper: ANN and linear regression. Non-linear parametric regression [47] is another technique that was considered. It should be noted, however, that to use non-linear regression, one needs to choose a parametrized non-linear model of the form $Y = f(X, \beta)$, where X is the predictors matrix, Y the values to be predicted, and β a parameters vector. The goal then is to find the optimal value of the parameters vector β that allows f to best fit the data. There are numerous families of functions from which f can be chosen: exponential functions, logarithmic functions, trigonometric functions, nth root functions, rational functions, polynomials of various degrees, etc. The first challenge is to find a suitable family of functions to express f, that will allow it to fit the data with an acceptable level of accuracy. This is not an easy task. All the non-linear models that were tried in this work resulted in much lower accuracy than the methods based on ANNs and linear regression. This is due to the fact that the chosen models were not adequate for the data at hand. Finding the right model is not easy, especially when many parameters are involved.

Neural networks on the other hand, are known for their ability to learn non-linear relations, without requiring a model of those relations as an input. The models obtained in this work, using neural networks, are in fact non-linear, and their accuracy is much higher than that of linear models. In cases where a model of the relationship between input and output is not known, neural networks can be a practical alternative to non-linear prediction.

4.5. Defect depth prediction using ANNs

This work explored the use of feedforward neural networks (FFNNs) [22]. Other types of neural networks will be considered in a future work. The dataset comprises around 1300 data items (input features and target output). Each data item corresponds to a cylindrical defect of a different size (radius and depth). The dataset is first partitioned into three separate sets: one for training, one for cross-validation, and one for testing. The partitioning is performed using random sampling; the indices of the set are first shuffled through a random permutation. Then the first 70% are assigned to the training set, the next 15% to the validation set, and the remaining 15% to the test set. The neural network is trained using the Early Stopping Cross-validation technique [43] which can be summarized in Fig. 15.

4.6. Neural network size and architecture

A number of parameters can be fine-tuned to obtain the optimal neural network configuration for the task at hand. These include parameters such as:

1. The number of hidden layers, and the size of each layer.
2. The error performance function (e.g., mean squared error, sum squared error, etc.)
3. The training algorithm (e.g., gradient descent [22,38], Levenberg–Marquardt [30,33], etc.)
4. The transfer functions [22,38] used in the hidden layer neurons (e.g., log sigmoid, hyperbolic tangent sigmoid, etc.)

The experiments presented in this paper sought to optimize the ANN with respect to the number of hidden layers and their sizes, and kept the other parameters fixed as follows:

1. Error performance function: mean squared error.
2. Training algorithm: Levenberg–Marquardt.
3. Transfer function: log sigmoid.

It might be useful to conduct an optimization search with respect the parameters above, but this is not in scope for this paper.

To find the optimal network size, an experiment was performed for ANNs with 1, 2, and 3 hidden layers, where each layer had a

[4] The signal is first normalized with respect to the maximum magnitude, and then normalized with respect to position. That is, the position of the two peaks are mapped to −1 and +1, and the signal is shrunk to fit on the [−1,1] interval. This provides a better way to compare signals on the same interval while preserving their overall shape.

```
Input: Dataset
Output: Trained ANN and error performance on test dataset
Initialize new ANN;
valError ⟵ +∞;                    /* MSE on validation vataset */
successiveFailsCounter ⟵ 0;       /* Counts how many times, in */
                                  /* a row, MSE on validation */
                                  /* dataset has increased */
maxFails ⟵ 6;                /* Denotes the max number of times */
          /* the validation error is allowed to decrease */
    /* before training ends.  It can be set to any value */
repeat
    Train ANN on training dataset only;
    valError ⟵ MSE of resulting ANN on validation dataset;
    Store new ANN configuration and valError ;    /* Information */
                                /* is appended to previous data */
    if valError > valError of previous round then
        successiveFailsCounter ++;
    end
until successiveFailsCounter = maxFails;
Among all ANN configurations tried in the repeat loop, find optimal
 ANN for which the validation error valError is minimum.
return optimal ANN and its MSE on the test dataset
```

Fig. 15. ANN training using Early Stopping Cross-validation [43].

number of neurons ranging from 5 to 100. Each of the ANN configurations above was used to analyze data from noiseless and noisy MFL signals with SNRs equal to 10 dB, 5 dB, and 3 dB, and the error performance was recorded. All experiments were done in MATLAB using the Neural Networks Toolbox [7]. The optimal network sizes obtained from those experiments are shown in Table 2. The depth prediction experiments presented in the remainder of this paper use the optimal networks sizes shown in Table 2. The results of those experiments are given in Section 5.3.

4.7. Defect depth prediction using linear regression

For the sake of comparison, the same datasets from the previous sections were used to predict defect depths using linear regression (LR) [22]. To make the comparison as precise as possible, the same partitions (training, validation, and testing) used in the ANN experiments, were also used for linear regression. The training datasets were used to compute the linear regression models, and the test datasets to compute the error performance of the linear regression. The results of the linear regression, as well as comparison with the ANN performance are given in Section 5.3.

5. Performance results

5.1. Performance criterion

The performance criterion adopted in this paper is *Prediction Accuracy @80% Certainty*, which is defined as the half width of the error interval that the prediction method can guarantee for at least 80% of the test dataset. For example, a prediction accuracy @80% of ±10% means that the prediction error, for at least 80% of the dataset, is in the range ±10% of the real defect depth. Accuracy at higher or lower levels of certainty (e.g., @95% or @70%) can also be considered, depending on the sensitivity of the application. This criterion is used to evaluate the accuracy of defect length and defect depth predictions.

5.2. Performance results of defect length prediction

Table 3 shows the accuracy @80% certainty of defect length predictions based on the WT technique. The accuracy is given for noisy and noiseless signals. The tables in Appendix A give the length sizing accuracy at 70% and 90% certainty. As Table 3 shows, the length sizing accuracy of the WT-based technique is almost perfect for noiseless signals, but decreases for noisy signals. To improve the

Table 2
Optimal ANN sizes and MSEs for noisy and noiseless data sets.

	1 hidden layer	2 hidden layers	3 hidden layers
Noiseless	[40]/4.8e−05	[25,5]/8.3e−06	[45,5,25]/4.7e−06
SNR = 10 dB	[65]/0.0271	[15,5]/0.0181	[25,65,5]/0.0165
SNR = 5 dB	[85]/0.0285	[15,25]/0.0253	[45,45,5]/0.0271
SNR = 3 dB	[45]/0.0175	[45,35]/0.0172	[5,65,25]/0.0170

Table 3
Length prediction accuracy @80% certainty.

	Length accuracy @80% certainty			
	WT alone	WT + LR	WT + 1-lay. ANN	WT + 2-lay. ANN
Noiseless	±2%	±2%	±1%	±2%
SNR = 10 dB	±7%	±4%	±3%	±2%
SNR = 5 dB	±20%	±7%	±5%	±5%
SNR = 3 dB	±39%	±16%	±8%	±11%

Table 4
Depth prediction accuracy @80% certainty.

	Depth accuracy @80% certainty		
	2-Layer ANN	3-Layer ANN	Linear regression
Noiseless	<±1%	<±1%	±25%
SNR = 10 dB	±10%	±9%	±35%
SNR = 5 dB	±13%	±14%	±40%
SNR = 3 dB	±11%	±12%	±26%

Table 5
Best accuracy results achieved.

	Accuracy @80% certainty	
	Length prediction	Depth accuracy
Noiseless	±1%	<±1%
SNR = 10 dB	±2%	±9%
SNR = 5 dB	±5%	±13%
SNR = 3 dB	±8%	±11%

length sizing accuracy for noisy signals, the defect lengths predicted by the WT technique were combined with features extracted from defect signals, and fed to machine learning techniques (ANNs and linear regression). More precisely, the features extracted in Section 4.4 were added to the defect lengths predicted by the Wavelet-based technique of Section 3.2. PCA was then applied to the dataset, thereby reducing the number of features from 34 to 7 or 10 depending on the noise level (c.f., Table 1). The projection of the dataset along the principal components was then fed to one-layer and two-layer ANNs, as well as linear regression.

As can be seen in Table 3, the application of machine learning techniques has drastically improved the length sizing accuracy, with the WT + 1-layer ANN combination giving the best results. It is worth noting here that applying the ML techniques to the WT-predicted defect lengths alone did not lead to any improvement in accuracy. Adding the extracted features produced the improvements shown in Table 3.

5.3. Performance results of defect depth prediction

Table 4 shows the accuracy @80% achieved by two-hidden-layer and three-hidden-layer ANNs, as well as the linear regression technique. All accuracy figures in Table 4 were computed on the test Dataset. The network sizes used for the two-hidden-layer and three-hidden-layer ANNs are the optimal ones, indicated in Table 2.

Figs. 16–18 show the depth prediction accuracy performance of 2-layer ANN, 3-layer ANN, and the linear regression technique, obtained for MFL signals with SNR = 10 dB. The accuracy is shown for different levels of certainty. The accuracy @80% certainty is highlighted in red. Tables showing the depth prediction accuracy at 70 and 90% accuracy, obtained for noiseless and noisy signals with SNRs = 10 dB, 5 dB and 3 dB, are given in Appendix B.

6. Discussion

The solution described in this work consists of two parts. The first accomplishes three main tasks. It detects and locates metal-loss defects in the MFL scan of a pipeline, and provides an estimate of the length of the opening of each of those defects. The second part builds upon those findings, and computes an estimate of the depth of each of the detected defects.

The above solution has been tested on MFL signals simulated using analytical models described in [16–18,29]. The tests were conducted both on noiseless and on noisy versions of the simulated signals. The noisy versions had signal to noise ratios ranging from 3 dB to 10 dB.

The first part of the solution (defect detection, location, and WT-based length sizing) has achieved almost perfect accuracy for noiseless signals. The accuracy of the WT technique was moderately affected for the noisy versions of the signals. This is due to the fact that noise affects the smoothness of the wavelet transform, and makes the WT surface more rugged and less regular. This makes it more difficult to distinguish local maxima (in the WT) corresponding to real defects, from those introduced by noise. To overcome this limitation, defect lengths predicted by the WT technique were combined with features extracted from the defect signals, and fed to machine learning techniques (ANNs and linear regression). This combination has drastically improved the length sizing accuracy as shown in Table 3.

The second part of the solution, which uses ANNs to analyze data from MFL signals, achieved a depth prediction accuracy @80% certainty of less than ±1% for noiseless signals, and ±10% to ±13% for noisy signals with SNRs equal to 3 dB, 5 dB and 10 dB. As shown in Table 4, the accuracy of the ANN-based method is neatly superior to that of linear regression. Table 5 provides a summary of the best accuracy results achieved in this paper (all methods included) both for length and depth prediction.

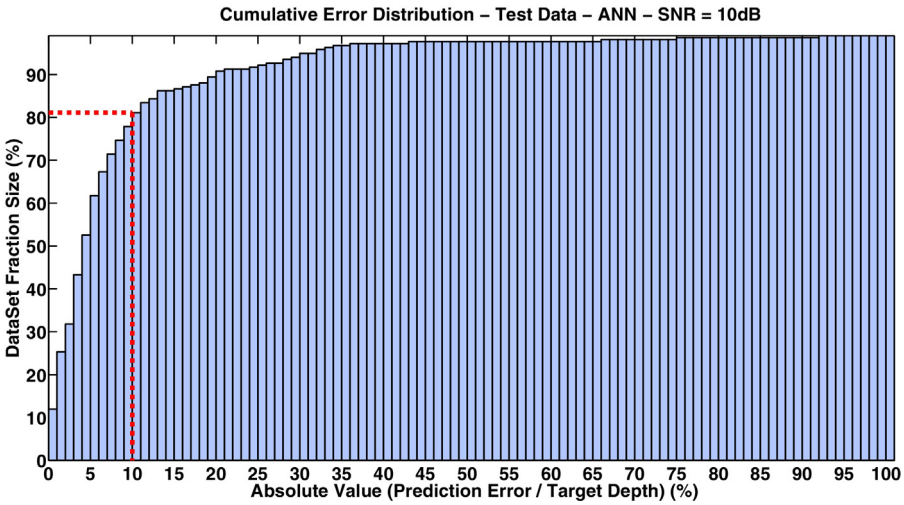

Fig. 16. Depth prediction accuracy of 2-layer ANN – SNR = 10 dB (The dotted lines indicates the accuracy @80%).

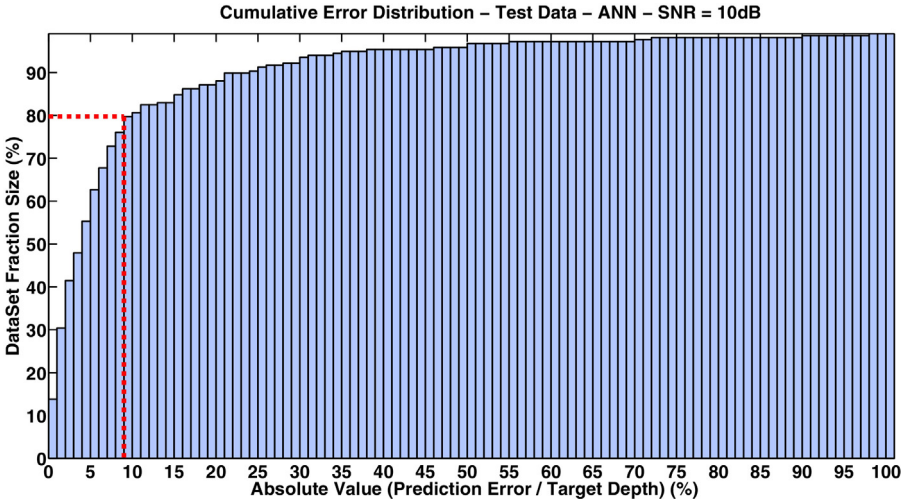

Fig. 17. Depth prediction accuracy of 3-layer ANN – SNR = 10 dB (The dotted lines indicates the accuracy @80%).

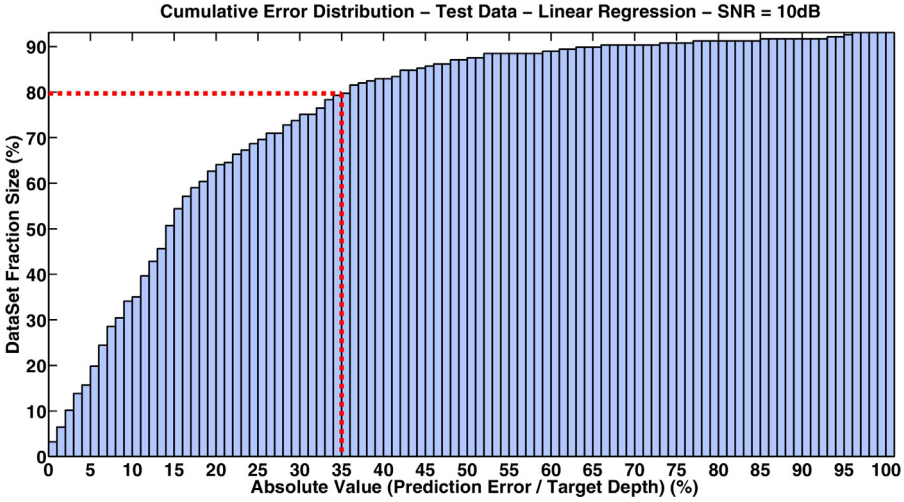

Fig. 18. Depth prediction accuracy of linear regression – SNR = 10 dB (The dotted lines indicates the accuracy @80%).

To further improve the prediction accuracy for noisy signals, the following measures will be explored:

- Using signal processing techniques to de-noise signals prior to the feature extraction step.
- Running the proposed solution again on MFL signals recorded at a lower lift-off (i.e., height at which the MFL signals are recorded). The MFL signals used in this work were simulated for a lift-off = 1 cm. MFL signals recorded or simulated at a lower lift-off have higher amplitudes and sharper features, and delineate defects much more closely.

7. Conclusions and future work

The goal of this work has been to detect, locate, and estimate the size of metal-loss defects from the MFL scans of oil and gas pipelines. The proposed method is based on pattern-adapted wavelets and artificial neural networks, and achieves high levels of accuracy and computational efficiency. The proposed solution can detect any pattern in the MFL signal that is designated as a reference pattern. In particular, it does not require knowledge of the analytical models of the defect shapes to be detected. Because of this flexibility, the proposed solution applies to a much wider range of defect shapes, even those for which analytical models are not known. Another feature of the proposed method is that defect detection and sizing are fully automated.

The results presented in this paper used the MFL signal of a cylindrical defect as a reference pattern. In a future work, other defect shapes (e.g., spherical, spheroidal, and cuboidal) will be used as reference patterns, and a comparative analysis will be conducted to determine which shape is best suited for the detection and sizing of naturally-occurring arbitrarily-shaped defects, such as surface corrosion. As highlighted in the previous section, various measures will be taken to further improve robustness to noise. The proposed solution will be also applied to real MFL data from operating pipelines, once such a data becomes available, and the results will be published.

Acknowledgement

The authors would like to thank Mr. Ibrahim Hachicha, from GE Oil & Gas, for his help in the early stages of this research, and for explaining the technology behind pipeline inspection tools. The authors would like also to thank Mr. Ahmed Layouni for his

help designing an efficient algorithm to search for local maxima in wavelet transform matrices.

This work was made possible by NPRP grant # [5-813-1-134] from the Qatar National Research Fund (a member of Qatar Foundation). The statements made herein are solely the responsibility of the authors.

Appendix A. Length prediction accuracy performance

Table A.6
Length prediction accuracy @70% certainty.

	Length accuracy @70% certainty			
	WT alone	WT + LR	WT + 1-lay. ANN	WT + 2-lay. ANN
Noiseless	<±2%	<±2%	<±1%	±1%
SNR = 10 dB	±6%	±3%	±3%	±2.5%
SNR = 5 dB	±12%	±5%	±3.5%	±4.5%
SNR = 3 dB	±21%	±11%	±6.5%	±8%

Table A.7
Length prediction accuracy @90% certainty.

	Length accuracy @90% certainty			
	WT alone	WT + LR	WT + 1-lay. ANN	WT + 2-lay. ANN
Noiseless	±8%	±5%	±3.5%	±2.5%
SNR = 10 dB	±12%	±5%	±5%	±5%
SNR = 5 dB	±40%	±10%	±7%	±9%
SNR = 3 dB	±65%	±22%	±11%	±15%

Appendix B. Depth prediction accuracy performance

Table B.8
Depth prediction accuracy @70%.

	Depth accuracy @70% certainty		
	2-Layer ANN	3-Layer ANN	Linear regression
Noiseless	<±1%	<±1%	±18%
SNR = 10 dB	±7.5%	±7.5%	±26%
SNR = 5 dB	±10%	±10%	±28%
SNR = 3 dB	±9%	±8.5%	±20%

Table B.9
Depth prediction accuracy @90%.

	Depth accuracy @90% certainty		
	2-Layer ANN	3-Layer ANN	Linear regression
Noiseless	±2.5%	<±1%	±56%
SNR = 10 dB	±20%	±21%	±66%
SNR = 5 dB	±22%	±24%	±90%
SNR = 3 dB	±16%	±19%	±46%

References

[1] A. Aharoni, Introduction to the Theory of Ferromagnetism, Oxford University Press, 1996.
[2] A. Al-Fahoum, I. Howitt, Combined wavelet transformation and radial basis neural networks for classifying life-threatening cardiac arrhythmias, Med. Biol. Eng. Comput. 37 (5) (1999) 566–573.
[3] American Society of Mechanical Engineers, ASME B31G – 1991 – Manual for Determining Remaining Strength of Corroded Pipelines, 1991, Retrieved April 2014: http://www.engineeringtoolbox.com/asme-d_7.html.
[4] Association of Oil Pipe Lines, Report on Shifts in Petroleum Transportation: 1990–2009, 2012, Retrieved April 2014: http://www.aopl.org.
[5] K.P. Balanda, H. MacGillivray, Kurtosis: a critical review, Am. Stat. 42 (2) (1988) 111–119.
[6] S.H.S. Barakat, Fault Detection, Classification, and Location in Underground Cables (Ph.D. thesis), Fayoum University, Egypt, 2014.
[7] M.H. Beale, M.T. Hag, H.B. Demuth, MATLAB Neural Network Toolbox™ – User's Guide, MathWorks, 2014.
[8] S. Beck, M. Curren, N. Sims, R. Stanway, Pipeline network features and leak detection by cross-correlation analysis of reflected waves, J. Hydraul. Eng. 131 (8) (2005) 715–723.
[9] S. Beck, J. Foong, W. Staszewski, Wavelet and cepstrum analyses of leaks in pipe networks, in: Progress in Industrial Mathematics, vol. 8 of Mathematics in Industry, Springer, 2006, pp. 559–563.
[10] J.P. Bigus, Data Mining with Neural Networks: Solving Business Problems from Application Development to Decision Support, McGraw-Hill, Inc., 1996.
[11] B.P. Bogert, M.J. Healy, J.W. Tukey, Quefrency analysis of time series for echoes: cepstrum, pseudo-autocovariance, cross-cepstrum and saphe cracking, in: Proceedings of the Symposium on Time Series Analysis, vol. 15, 1963, pp. 209–243.
[12] J.N. Bradley, C.M. Brislawn, T. Hopper, FBI wavelet/scalar quantization standard for gray-scale fingerprint image compression, in: SPIE Proceedings, Visual Information Processing II, vol. 1961, SPIE, 1993, pp. 293–304.
[13] Canadian Energy Pipeline Association, Protecting Pipeline Integrity – It is a Full-Time Job!, 2012, Retrieved April 2014: http://www.cepa.com/2012/09.
[14] Canadian Energy Pipeline Association, Facts About the Use of Energy Pipelines in Canada, 2013, Retrieved April 2014: http://www.cepa.com/library/factoids.
[15] I. Daubechies, Ten Lectures on Wavelets, Society for Industrial and Applied Mathematics, SIAM, 1992.
[16] S. Dutta, F. Ghorbel, R. Stanley, Dipole modeling of magnetic flux leakage, IEEE Trans. Magn. 45 (4) (2009) 1959–1965.
[17] S. Dutta, F. Ghorbel, R. Stanley, Simulation and analysis of 3-D magnetic flux leakage, IEEE Trans. Magn. 45 (4) (2009) 1966–1972.
[18] S.M. Dutta, Magnetic Flux Leakage Sensing: The Forward and Inverse Problems (Ph.D. thesis), Rice University, USA, 2008.
[19] M. Ermes, Methods for the Classification of Biosignals Applied to the Detection of Epileptiform Waveforms and to the Recognition of Physical Activity (Ph.D. thesis), Tampere University of Technology, Finland, 2009.
[20] M. Ghazali, W.J. Staszewski, J. Shucksmith, J.B. Boxall, S.B. Beck, Instantaneous phase and frequency for the detection of leaks and features in a pipeline system, Struct. Health Monit. 10 (4) (2011) 351–360.
[21] R. Glasius, A. Komoda, S.C. Gielen, Neural network dynamics for path planning and obstacle avoidance, Neural Netw. 8 (1) (1995) 125–133.
[22] S.O. Haykin, Neural Networks and Learning Machines, Prentice Hall, 2008.
[23] J.E. Jackson, A User's Guide to Principal Components. Wiley Series in Probability and Statistics, John Wiley & Sons, Inc., 2004.
[24] I.T. Jolliffe, Principal Component Analysis. Springer Series in Statistics, Springer, 2002.
[25] S. Kaitwanidvilai, C. Pothisarn, C. Jettanasen, P. Chiradeja, A. Ngaopitakkul, Discrete wavelet transform and back-propagation neural networks algorithm for fault classification in underground cable, in: Proceedings of the International Multiconference of Engineers and Computer Scientists, vol. II, 2011, pp. 996–1000.
[26] J. Khan, J.S. Wei, M. Ringner, L.H. Saal, M. Ladanyi, F. Westermann, F. Berthold, M. Schwab, C.R. Antonescu, C. Peterson, et al., Classification and diagnostic prediction of cancers using gene expression profiling and artificial neural networks, Nat. Med. 7 (6) (2001) 673–679.
[27] H.M. Kim, D.W. Jeong, S.H. Im, J.H. Park, J.S. Lee, G.S. Park, A study on the estimation of defect depth in MFL type NDT system, in: Proceedings of the 20th International Conference on the Computation of Electromagnetic Fields (COMPUMAG), 2015, p. PA6-8.
[28] N. Kohzadi, M.S. Boyd, B. Kermanshahi, I. Kaastra, A comparison of artificial neural network and time series models for forecasting commodity prices, Neurocomputing 10 (2) (1996) 169–181, Financial Applications, Part I.
[29] M. Layouni, S. Tahar, M.S. Hamdi, A survey on the application of neural networks in the safety assessment of oil and gas pipelines, in: IEEE Symposium on Computational Intelligence for Engineering Solutions (CIES), 2014, pp. 95–102.
[30] K. Levenberg, A method for the solution of certain problems in least squares, Q. Appl. Math. 2 (1944) 164–168.
[31] X. Ma, C. Zhou, I. Kemp, Interpretation of wavelet analysis and its application in partial discharge detection, IEEE Trans. Dielectr. Electr. Insul. 9 (3) (2002) 446–457.
[32] S. Mallat, A Wavelet Tour of Signal Processing, Academic Press, 2008.
[33] D.W. Marquardt, An Algorithm for Least-Squares Estimation of Nonlinear Parameters, SIAM J. Appl. Math. 11 (2) (1963) 431–441.
[34] MATLAB, Version 7.12.0 (R2011a), The MathWorks Inc., 2011.
[35] J.C.H. Mejia, Characterization of Real Power Cable Defects by Diagnostic Measurements (Ph.D. thesis), Georgia Institute of Technology, USA, 2008.
[36] H. Mesa, Adapted wavelets for pattern detection, in: Progress in Pattern Recognition, Image Analysis and Applications, vol. 3773 of Lecture Notes in Computer Science, Springer-Verlag, 2005, pp. 933–944.
[37] M. Misiti, Y. Misiti, G. Oppenheim, J.-M. Poggi, Wavelets and Their Applications, Wiley-ISTE, 2007.
[38] G. Montavon, G. Orr, K.-R. Müller, Neural Networks: Tricks of the Trade, Vol. 7700 of Lecture Notes in Computer Science – Computer State-of-the-Art Surveys, Springer, 2012.

[39] Y.-S. Moon, S.-K. Lee, Gas leakage in buried gas pipe based on wavelet analysis for vibro-coustic signal in a long duct, J. Intell. Mater. Syst. Struct. 22 (5) (2011) 387–399.
[40] J. Muggleton, M. Brennan, Leak noise propagation and attenuation in submerged plastic water pipes, J. Sound Vibr. 278 (3) (2004) 527–537.
[41] S. Mukhopadhyay, G. Srivastava, Characterisation of metal loss defects from magnetic flux leakage signals with discrete wavelet transform, NDT&E Int. 33 (1) (2000) 57–65.
[42] N.R. Pearson, M.A. Boat, R.H. Priewald, M.J. Pate, J.S. Mason, A study of MFL signals from a spectrum of defect geometries, in: Proceedings of the 18th World Conference on Nondestructive Testing, 2012, pp. 1546–1553.
[43] L. Prechelt, Automatic early stopping using cross validation: quantifying the criteria, Neural Netw. 11 (4) (1998) 761–767.
[44] R.H. Priewald, P.D. Ledger, N.R. Pearson, J.S. Mason, Uncertainties of MFL signal inversion and worst-case defect depth estimation using a numerical model, in: Electromagnetic Nondestructive Evaluation (XVI), vol. 38 of Studies in Applied Electromagnetics and Mechanics, 2014, pp. 55–65.
[45] R.B. Randall, Frequency Analysis, Brül & Kjor, 1987.
[46] M. Ravan, R. Amineh, S. Koziel, N. Nikolova, J. Reilly, Sizing of 3-D arbitrary defects using magnetic flux leakage measurements, IEEE Trans. Magn. 46 (4) (2010) 1024–1033.
[47] G. Seber, A. Lee, Linear Regression Analysis. Wiley Series in Probability and Statistics, Wiley, 2012.
[48] G. Strang, G.J. Fix, An Analysis of the Finite Element Method. Prentice-Hall Series in Automatic Computation, Wellesley-Cambridge, 2008.
[49] M. Unser, A. Aldroubi, A review of wavelets in biomedical applications, Proc. IEEE 84 (4) (1996) 626–638.
[50] J. Urbanek, T. Barszcz, T. Uhl, W. Staszewski, S. Beck, B. Schmidt, Leak detection in gas pipelines using wavelet-based filtering, Struct. Health Monit. 11 (4) (2012) 405–412.
[51] Z. Zhang, D. Fan, Y. Sun, Fault detection in sub-sea pipelines using discrete wavelet transform method, in: Proceedings of the Twentieth International Offshore and Polar Engineering Conference, 2010, pp. 109–114.